JOURNAL OF ENVIRONMENTAL SCIENCES 124 (2023) 300–309

Available online at www.sciencedirect.com

ScienceDirect

www.elsevier.com/locate/jes

JES JOURNAL OF ENVIRONMENTAL SCIENCES

www.jesc.ac.cn

Through converting the surface complex on TiO_2 nanorods to generate superoxide and singlet oxygen to remove CN^-

Laiqi Zhang[1,2], *Ridha Djellabi*[3], *Peidong Su*[2], *Yan Wang*[2,*], *Jianling Zhao*[1,*]

[1] *School of Materials Science and Engineering, Hebei University of Technology, Tianjin 300401, China*
[2] *Key Laboratory of Drinking Water Science and Technology, Research Center for Eco-Environmental Sciences, Chinese Academy of Sciences, Beijing 100085, China*
[3] *Dip. Chimica and INSTM-UdR Milano, Università degli Studi di Milano, Via Golgi, 19 20133 Milano, Italy*

ARTICLE INFO

Article history:
Received 18 May 2021
Revised 16 August 2021
Accepted 30 August 2021
Available online 2 February 2022

Keywords:
TiO_2
Photo-electrocatalytic
Peroxymonosulfate activation
Cyanide removal
Water remediation

ABSTRACT

Cyanide (CN^-) is extensively used in the process of plating devices and for surface treatment in the electroplating industry and is extremely hazardous to humans and the environment. Peroxymonosulfate (PMS)-based advanced oxidation processes (AOPs) hold considerable promise for CN^- removal. However, the activity of sulfate radical and hydroxyl radical generated in the PMS activation process is low in the base condition, leading to a drop in its efficiency in CN^- removal. Thus, a photo-electrocatalytic system (PEC), developed using a TiO_2 photoanode and a carbon aerogel cathode, was used to activate PMS for the removal of CN^- from wastewater through the generation of radicals and non-radicals. The PEC/PMS system could effectively remove CN^-, with the removal efficiency reaching 98.5% within 2 min, when PMS concentration was at the 0.25 mmol/L level, and the applied bias voltage was -0.5 V. The main active species in the PEC/PMS system were superoxide radicals and singlet oxygen, which was proved through electron paramagnetic resonance detection and quenching experiments. Results obtained through *in-situ* Raman measurements, photocurrent tests, and electrochemical impedance spectroscopy measurements indicated that the TiO_2 could activate PMS to generate active species. Following many cycles of experimentation, it was discovered that the system displayed high catalytic performance and possessed satisfactory stability to remove CN^- economically and efficiently.

Introduction

Cyanide (CN^-) is extensively used in the process of plating devices and for surface treatment in the electroplating industry due to its robust complexing ability with metal ions (Adams et al., 2020; Monser and Adhoum, 2002), leading to a large concentration of residual CN^- being found in wastewater generated from the electroplating process. The presence of CN^- in waters even at low concentration of 0.04–0.1 mg/L damages significantly fish and other aquatic organisms. Untreated electroplating wastewaters contain usually high amounts of CN^-, even much higher than the recommended concentration, which poses a serious threat to the environment and human health. Therefore, the intensification of technologies towards CN^- removal from wastewater is

* Corresponding authors.
E-mails: yanwang@rcees.ac.cn (Y. Wang), hebutzhaoj@126.com (J. Zhao).

https://doi.org/10.1016/j.jes.2021.08.054
1001-0742/

very recommended to maintaining water security and human health.

A variety of methods have been developed to eliminate CN^- from wastewater including alkaline chlorination (Lv et al., 2015), electrodialysis (Zheng et al., 2015), electrocatalysis (Wang et al., 2017), and photo-electrocatalysis (Mao et al., 2019; Dong et al., 2021; Tian et al., 2018). Additionally, the persulfate-based advanced oxidation processes (AOPs) enable the efficient degradation of CN^- due to the strong oxidation ability of sulfate radicals (SO_4^{-}•) produced in the process (Zhu et al., 2019; Deng et al., 2018). Peroxydisulfate (PDS) and peroxymonosulfate (PMS) are two typical persulfates, with PMS possessing the potential to be readily activated to yield SO_4^{-}• due to its asymmetric structure (Duan et al., 2016; Song and Liu, 2018), thus garnering more attention than PDS. SO_4^{-}• possesses high oxidation potential (2.8–3.0 eV) and a long half-life (30–40 μsec) (Wang et al., 2018), resulting in its high efficacy in the degradation of pollutants. Apart from SO_4^{-}•, PMS can be converted and used to produce other strong oxidizing active species such as hydroxyl radicals (•OH) (Duan et al., 2018; Gao et al., 2018), superoxide radicals (O_2^{-}•) (Han et al., 2020; Li et al., 2020), and singlet oxygen ($^1O_2$) (Duan et al., 2020; Fan et al., 2019), all of which could be effectively used for the degradation of pollutants in wastewater.

The activation of PMS to generate active species is dependent on external factors, with the commonly used methods at present being energy transfer (including heat, UV, and ultrasound) and transition metal activation (Chen et al., 2019; Ao et al., 2018; Wang and Wang, 2018). The SO_4^{-}• and •OH generated through these processes could be used to remove organic pollutants. However, SO_4^{-}• and •OH could also be expended by other species, such as anion Cl^-, HCO_3^-, CO_3^{2-}, and NO_3^- (Jawad et al., 2020), forming Cl•, HCO_3^{-}•, CO_3^{2-}•, and NO_3^{-}•, and the oxidizing capacity of these newly formed radicals would be too low to remove pollutants. Moreover, researchers would also need to consider the drawbacks to this method such as excessive energy inputs and transition metal ions leaching out. Therefore, it was imperative that an economical and efficient method to activate PMS be developed. Recent research indicated that the use of photoelectric catalysts and carbon materials was an excellent mode of activating PMS to produce non-radicals (Chen et al., 2021; Qin et al., 2020). Among the photoelectric catalysts, TiO_2 was one of the most significant semiconductor photocatalysts due to its light corrosion resistance and photochemical stability. Previous study indicated that PMS activation could be enabled through a ligand-to-metal charge transfer (LMCT) mechanism (Joa et al., 2018). Although carbonaceous materials have showed excellent catalytic PMS activation, among them carbon aerogel (CA) based materials have showed many unique properties due to the three-dimensional network structure which could intensity the catalytic efficiency (Wang et al., 2013).

Having been enlightened by previous researchers, a photoelectrocatalytic (PEC) system, constructed using TiO_2 as the photoanode and CA as the cathode, was used to activate PMS and achieve CN^- removal in this study. The generation of non-radicals during the PMS activation process in the inherent strong base condition (CN^- would escape into the air when the pH value was as low as 9) via conversion of surface complexes, was expected. The removal process was optimized by studying the influence of different PMS concentrations, photocatalysis, electrocatalysis, and the applied bias voltage on the activation of PMS, and then the reaction kinetic in the process of CN^- removal using the PEC/PMS method was explored. Furthermore, the removal mechanism and active species were studied by conducting electron paramagnetic resonance (EPR) tests and quenching experiments. Finally, the effect of TiO_2 on PMS activation was analyzed using the *in-situ* Raman test, photocurrent density, and electrochemical impedance spectroscopy (ESI). Overall, this work offered an emerging and promising method to activate PMS and generate active species to treat CN^--contaminated wastewater.

1. Materials and methods

1.1. Reagents

Tetra-*n*-butyl titanate ($C_{16}H_{36}O_4Ti$, analytical reagent (AR), 98.0 wt.%), hydrochloric acid (HCl, guaranteed reagent (GR), 36.0–38.0 wt.%), absolute ethanol (C_2H_5OH, GR, 99.0 wt.%), chloramine T trihydrate ($C_7H_7ClNNaO_2S•3H_2O$, AR, (Cl) 24.0 at.%), isonicotinic acid ($C_6H_5NO_2$, chemical pure (CP), 98.0 wt.%), barbituric acid ($C_4H_4N_2O_3$, AR, 99.0 wt.%), potassium monopersulfate triple salt (PMS, $KHSO_5$, 47.0 wt.%), resorcinol ($C_6H_6O_2$, AR, 99.0 wt.%), formaldehyde (CH_2O, 37.0 wt.%), sodium carbonate (Na_2CO_3, AR, 98 wt.%), sodium cyanide (NaCN, AR, 98.0 wt.%) and sodium hydroxide (NaOH, AR, 96.0 wt.%) were bought from Sinopharm Chemical Reagent Co., Ltd; Methanol (CH_3OH, high pressure liquid chromatography (HPLC) grade ≥ 99.9 wt.%) and acetone (C_3H_6O, AR, 98.0 wt.%) were purchased from Thermo Fisher scientific Co., Ltd.; Nessler reagent (AR), were obtained from Sigma Reagent Co., Ltd.; Potassium sodium tartrate tetrahydrate ($C_4H_4O_4KNa•4H_2O$, AR, 98.0 wt.%) was purchased from shanghai Macklin biochemical co., Ltd. All the reagents have not been further purification.

1.2. Preparation

1.2.1. Preparation of TiO_2 nanorods (NRs)

The synthesis of TiO_2 NRs by hydrothermal method was carried out based on previous report (Xie et al., 2013): 45 mL of HCl and 45 mL of ultrapure water were added into a beaker and stir for 5 min. Subsequently, 1.5 mL of tetra-*n*-butyl titanate was dropwise added to the mixed solution, and the mixture was transferred to a polytetrafluoroethylene reactor after thorough stirring. Then the clean fluorine-doped tin oxide (FTO) glass was immersed in the mixture obliquely with the conductive surface facing up, the reactor was transferred to an oven, and reacted at 150°C for 5 hr. During the reaction, TiO_2 will grow on the conductive surface of the FTO glass and cool to 20–25°C after the reaction. Then take out the FTO glass grown with TiO_2, rinse it with ultrapure water 3 times, and dry it naturally to obtain pure TiO_2. After drying, the FTO glass grown with TiO_2 was placed in a muffle furnace at 500°C and calcined for 2 hr at a heating rate of 2.5°C/min to obtain TiO_2 NRs.

1.2.2. *Preparation of CA*

CA was synthesized using the procedure reported in previous study (Wang et al., 2013). Resorcinol (55 g) was added to 98.5 mL of ultrapure water in a beaker, the mixture was stirred for 30 min. Formaldehyde (72.5 mL) and 4.24 g/L Na_2CO_3 (10 mL) were sequentially added and stirred for 30 min. Afterwards, the mixture was transferred to the prepared mold, and then the mold was wrapped with plastic wrap, and placed in the oven. It was reacted at 30 and 50°C for 1 day, respectively, and at 90°C for 3 days. Then, the plastic wrap was removed and the cured material was taken out, sand the material and soaked it in acetone for 3 days (the acetone needs to be replaced every day). After that, take out the material and place it in a fume hood to dry naturally. The dried material was put into a tube furnace with the protection of N_2 to carbonization at 950°C for 4 hr and the heating rate is 2.5°C/min. Then it was cooled to 20–25°C to obtain black solid CA.

1.3. *Experimental procedure*

NaCN solution (44.4 mg/L, 100 mL) was placed into the reactor with magnetic stirring, then adjusted the pH using 10 g/L and 1.0 g/L NaOH and kept the pH around 12. The PEC/PMS system was constructed with TiO_2 as the counter electrode, CA as the working electrode and calomel electrode as the reference electrode. The distance between the lamp and the reactor was kept 10 cm. A 300 W luminous power Xe lamp (Perfect Light technology Co., LTD, Beijing) was used as source for light. Sodium chloride (NaCl) and PMS were added to the NaCN solution, respectively, to study the effect of different additives on the degradation of cyanide. And the effects of different concentrations of PMS, applied bias and photocatalysis were studied separately. Sample (1.0 mL) was taken at 0, 0.3, 0.6, 1, 2, 5, and 10 min to detect the CN^- concentration.

1.4. *Analytical methods*

1.4.1. *CN^- concentration detection*

The concentration of CN^- was detected by isonicotinic acid-barbituric acid UV-Vis spectrophotometry (Wang et al., 2017; Gao et al., 2013). Under weak acid conditions, CN^- can react with chloramine-T to form cyanogen chloride, which then react with isonicotinic acid to form glutaraldehyde. The glutaraldehyde can form a blue-violet complex with barbituric acid, and the chroma of the complex is proportional to the concentration of CN^- within a certain range. The concentration of CN^- can be calculated through the calibration curve.

1.4.2. *CNO^- concentration detection*

CNO^- can be hydrolyzed to carbonate and ammonium under acidic conditions, so we can detect the concentration of ammonium to indirectly analyzed the concentration of CNO^- through the Nesslerization method (Guo et al., 2019).

1.4.3. *Free radicals' detection*

Free radicals were detected by electron paramagnetic resonance (EPR) (A300-10/12, Bruker Co., Ltd., German) and analyzed the signal peaks. The capture of $SO_4^{-}\bullet$, $\bullet OH$, and $O_2^{-}\bullet$ was 5,5-dimethyl-1-pyrroline-N-oxide (DMPO), and the capture of $^1O_2$ was 2,2,6,6-tetramethyl-4-piperidone hydrochloride (TEMP).

Water (100 mL) was placed into the reactor with magnetic stirring, then adjusted the pH using 10 g/L and 1.0 g/L NaOH and kept the pH around 12. The PEC/PMS system was constructed with TiO_2 as the counter electrode, CA as the working electrode and calomel electrode as the reference electrode, and then PMS was added to the solution. Under light irradiation condition, 30 μL solution was measured at 0, 1, 5, and 10 min, respectively. DMPO was added to the solution to captured $SO_4^{-}\bullet$ and $\bullet OH$. TEMP was added to another 30 μL solution at 0, 1, 5, and 10 min to captured $^1O_2$. All mixtures were placed in the instrument to detected.

Based on the above operation, we changed the water to methanol to obtained the peaks of $O_2^{-}\bullet$, and DMPO was added to the 30 μL of solution at 0, 1, 5, and 10 min to captured $O_2^{-}\bullet$; TEMP was added to another 30 μL of solution to captured $^1O_2$.

1.5. *Characterization*

The microstructure of catalyst was characterized by scanning electron microscopy (SEM, SU8010, HITACHI, Japan). The phase composition of catalyst was measured by X-ray diffraction (XRD, X'Pert 3 powder, Panalytical X'Pert Pro, Netherlands) with Cu $K\alpha$ radiation ($\lambda = 1.5418$ Å). X-ray photoelectron spectroscopy (XPS) measurements were recorded on a PHI-5300 Perkin–Elmer ESCA (USA) system operate at Al $K\alpha$ source. *In-situ* Raman measurements were performed at room temperature using a Raman spectrometer (HR800, Horiba Scientific, France) with an excitation wavelength 514 nm. The electrochemical characterization including electrochemical impedance spectroscopy (EIS) measurements and photocurrent density test were taken on a CHI 660D electrochemical analyzer (Shanghai Chenhua Instruments Co., Ltd, Shanghai, China) using a standard three-electrode system.

2. Results and discussion

2.1. *Characterization of TiO_2 NRs*

The microstructure of fresh TiO_2 NRs was analyzed using SEM and the results are showed in **Fig. S1a**. The SEM images revealed that TiO_2 NRs covered the surface of the FTO glass and were tetragonal in shape with square top facets. Such a structure could engender many active sites for catalysis, which was a desirable condition for PEC applications (Cho et al., 2011). The phase structure of fresh TiO_2 NRs was characterized by XRD (**Fig. S1b**). The phase structure was consistent with the rutile TiO_2 phase, and the peaks located at 2θ of 36.1°, 41.2°, 62.7°, 69.0°, and 69.8° corresponded to the reflection planes (101), (111), (002), (301), and (112) of TiO_2, respectively. **Fig. S2a** displays the XPS survey spectra of TiO_2, and the peaks at approximately 284, 460, and 530 eV were attributable to C 1s, Ti 2p, and O 1s, respectively. The high-resolution O 1s spectrum has two peaks located at 529.9 and 531.6 eV (**Fig. S2b**), with the first peak corresponding to the binding Ti-O-Ti (Akhavan and Ghaderi, 2010). The second peak at 531.6 eV can be assigned to the -OH in -Ti(OH)-O-Ti-(OH)-, which was beneficial in forming the complex on the TiO_2 surface (Hoffmann et al., 1995). **Fig. S2c** demonstrates the high resolution XPS spectrum of Ti 2p,

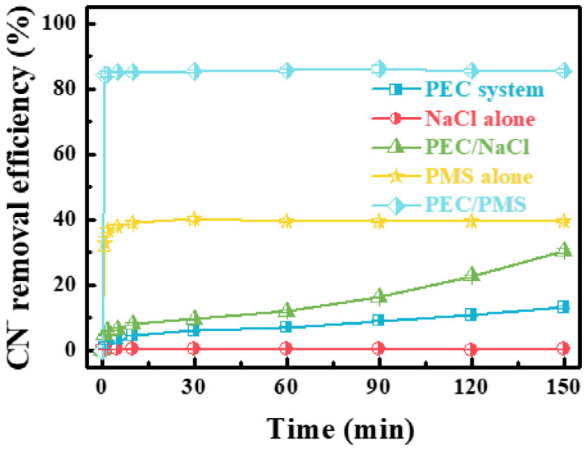

Fig. 1 – Removal efficiency of CN^- in presence of NaCl alone, peroxymonosulfate (PMS) alone, photoelectrocatalysis (PEC) system, PEC/NaCl and PEC/PMS system. Reaction conditions: [CN^-] = 44.4 mg/L, applied bias voltage = -1.2 V, pH = 12. 0 and light.

with the two peaks of Ti indicating the state of Ti^{4+} in the TiO_2 NRs (Ye et al., 2017).

2.2. *Effect of different additives on CN^- removal efficiency*

NaCl can be converted to active chlorine radicals during electrolysis which was used widely in industrial processing Sasidharan Pillai and Gupta, 2016). To oxidative role of PMS and NaCl towards CN^- removal was studied comparatively. In addition, CN^- removal was investigated in different systems including PEC, PEC/NaCl, and PEC/PMS. As can be observed in Fig. 1, a slight removal of CN^- was apparent within 150 min when NaCl alone was added, while in the presence of PMS alone, the CN^- removal efficiency stood at 38.1% within 10 min. In a separate PEC system, the CN^- removal efficiency was 17.0% within 150 min, and it was 30.0% in the PEC/NaCl system and 85.7% in the PEC/PMS system, respectively. The hypothesis drawn based on the above results was that with the mere addition of NaCl, the relative stability of NaCl failed to generate effective active radicals that were required to remove CN^-. While PMS alone was added, the CN^- removal efficiency increased to 38.1% since PMS could be catalyzed by OH^- to generate active species. As for the PEC system, the CN^- removal efficiency was only 17.0%, which could be attributed to the low activity of •OH under alkaline conditions (Sun et al., 2018; Yang et al., 2013), although the photoanode TiO_2 could produce a large amount of •OH under light radiation. With the PEC/NaCl system, chloride ions (Cl^-) were oxidized by •OH to generate active chlorine, such as Cl• and ClO^-. The conversion of chloride ions has been denoted in Eqs. (1)-(4). Active chlorine was favorable to the removal of CN^- (Tian et al., 2016). The reason for the PEC/PMS system obtaining a high CN^- removal efficiency of 85.7% was possibly because the PEC system could efficiently activate PMS to remove CN^-.

$$OH + Cl^- \rightarrow OH^- + Cl \quad (1)$$

$$Cl^- - e^- \rightarrow Cl \quad (2)$$

$$2Cl \rightarrow Cl_2 \quad (3)$$

$$Cl_2 + 2OH^- \rightarrow Cl^- + ClO^- + H_2O \quad (4)$$

2.3. *Effect of factors on PMS activation to remove CN^-*

To analyze the effect of PEC on PMS activation, the effect of some parameters on CN^- removal was studied (Fig. 2). When the PMS concentrations increased from 0.10 mmol/L, 0.25 mmol/L, 0.50 mmol/L to 1.00 mmol/L, the CN^- removal efficiency rose from 26.4%, 38.1%, 66.0% to 95.9% (Fig. 2**a**). Compared to the system that used only PMS, the increase in CN^- removal efficiency was more obvious in the photocatalysis (PC)/PMS, electrocatalysis (EC)/PMS, and PEC/PMS systems, ascending from 26.4% for the PMS system to 51.1%, 58.2%, and 63.4% for the PC/PMS, EC/PMS, and PEC/PMS systems respectively, with a PMS concentration level of 0.10 mmol/L (Fig. 2**b**), and ascending from 38.1% for the PMS system to 69.1%, 79.1%, and 85.7% for the PC/PMS, EC/PMS, and PEC/PMS systems, respectively, when the PMS concentration was at 0.25 mmol/L (Fig. 2**c**). The CN^- were completely removed in PC/PMS, EC/PMS, PEC/PMS system when the PMS concentrations were 0.50 and 1.00 mmol/L (**Fig. S3a** and **b**). These results indicated that the CN^- removal efficiency increased with an increase in PMS concentration, and the presence of light and applied bias voltage could activate PMS to further improve CN^- removal efficiency. Thus, it was inferred that (1): OH^- could be oxidized by the hole (h^+) generated via TiO_2 with the presence of light to form •OH to co-effect CN^- removal; (2): TiO_2 would interact with PMS to generate active species in the presence of light. As established by previous studies (Qin et al., 2020; Sun et al., 2014), carbon materials could activate PMS to remove pollutants from wastewater. Therefore, in the EC/PMS system, a part of PMS would be activated by the CA cathode to generate active species for the removal of CN^-. Additionally, CN^- removal efficiency of the PEC/PMS system with differing applied bias voltage has been illustrated in Fig. 2**d**. When the applied bias voltage was -1.2 V, the CN^- removal efficiency was 85.7%, while when the applied bias voltage was -0.5 and -2.0 V, CN^- removal efficiency increased to 98.5% and 99.6%, respectively. The effect of the applied bias voltage on CN^- removal could be attributed to the activation of PMS by a photoanode and cathode. A small portion of the PMS would be adsorbed and activated by the cathode CA when the applied bias voltage was low. The impact that the cathode had on the activation of PMS diminished with an amplification in the applied bias voltage due to the PMS as well as anions moving to the photoanode when the applied bias voltage was high. The competitive adsorption of anions and PMS onto the TiO_2 surface meant that TiO_2 could only activate PMS partially, leading to it possessing the lowest CN^- removal efficiency. What was interesting to note was that when the applied bias voltage increased to -2.0 V, the CN^- removal efficiency climbed to 99.6%, which could be ascribed to the effect engendered by the photoanode TiO_2.

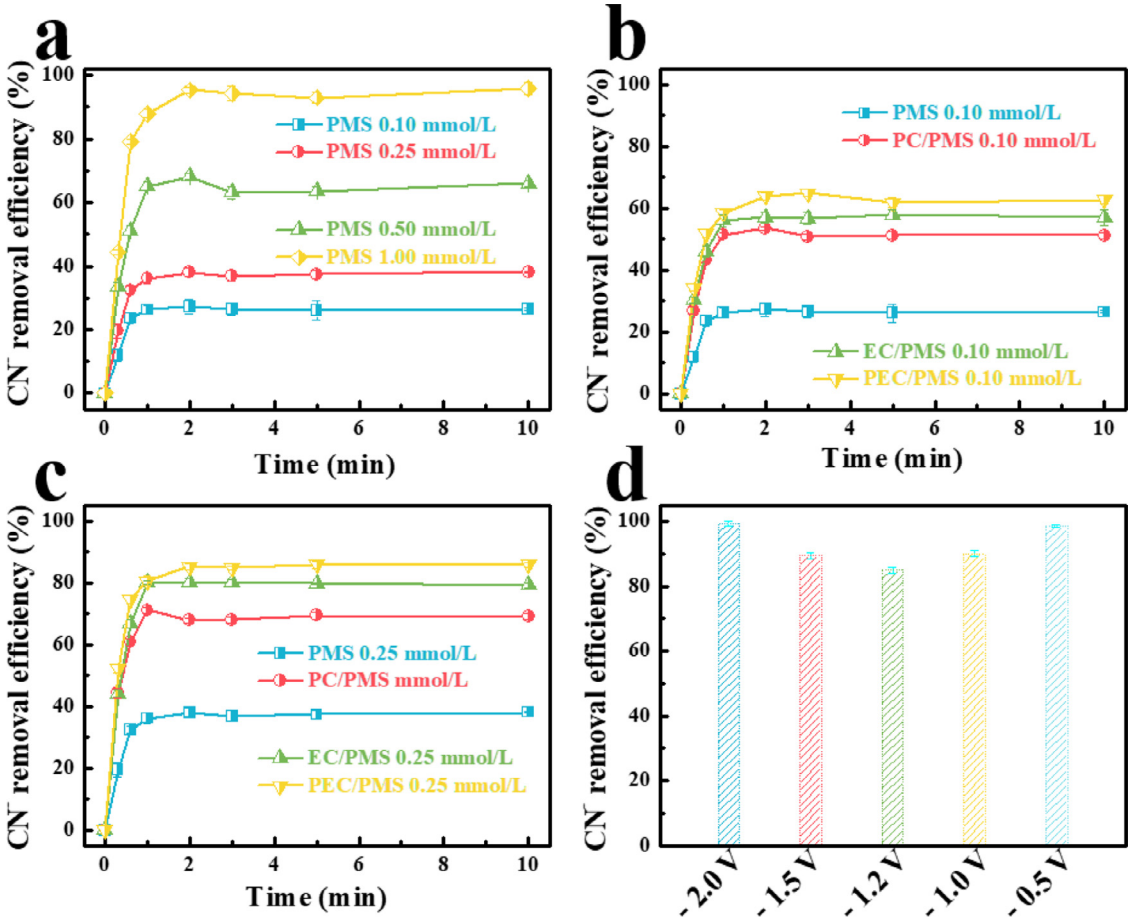

Fig. 2 – CN^- removal efficiency at (a) different PMS concentration, (b) 0.10 mmol/L PMS with different system, (c) 0.25 mmol/L PMS with different system and (d) effect of different applied bias voltage on CN^- removal. Reaction conditions: [CN^-] = 44.4 mg/L, applied bias potential = -1.2 V, pH = 12. 0 and light. PC: photocatalysis; EC: electrocatalysis.

2.4. *CN^- removal mechanism*

EPR free radical detection and a series of quenching experiments were performed to study the mechanism of CN^- removal. The findings have been displayed in Fig. 3**a** and **b**. Unlike the traditional PMS activation mechanisms, $SO_4^{-}\bullet$ and ●OH were not detected in the PEC/PMS system. Moreover, although a strong signal of DMPO-O_2 was detected, the intensity of the signal decreased with the passage of time, indicating that $O_2^{-}\bullet$ was the active species in the CN^- removal process. Apart from $O_2^{-}\bullet$, an EPR test also detected the signal of 2,2,6,6-tetramethylpiperidinooxy (TEMPO), indicating that $^1O_2$ was also active in CN^- removal, with the perceived change in the intensity of the signal of $^1O_2$ over time being similar to that of $O_2^{-}\bullet$. As is commonly known, it is possible to generate •OH from TiO_2 through h^+, and this has been proved through the experiments discussed above; however, no indication of DMPO-OH was detected post the addition of PMS (not illustrated). The hypothesis for this outcome was that the PMS would react with TiO_2, leading to the dissipation of •OH. Quenching experiments were carried out on the PEC/PMS system using an applied bias voltage of -0.5 V and a PMS concentration of 0.25 mmol/L. The potentially active species during experimentation on CN^- removal were primarily $SO_4^{-}\bullet$, ●OH, $^1O_2$, $O_2^{-}\bullet$, and h^+, and the scavengers were methanol, *tert*-butanol, *L*-histidine, *p*-benzoquinone, and ethylenediaminetetraacetic acid disodium salt (EDTA-2Na), respectively (Wang and Wang, 2020; Clifton and Huie, 1989). The scavengers and their corresponding rate constants have been recorded in Table 1. The results of the quenching experiments have been illustrated in Fig. 3**c**. After having added methanol to quench $SO_4^{-}\bullet$ and *tert*-butanol to quench ●OH, hardly any change was observed in the CN^- removal efficiency, thus confirming that $SO_4^{-}\bullet$ and ●OH were not active species for CN^- removal. When *L*-histidine was added to quench $^1O_2$, the CN^- removal efficiency fell from 98.5% to 76.3%, indicating that $^1O_2$ was one of the active species for CN^- removal. A point to be noted is that the CN^- removal rate decreased from 98.5% to 37.4% after the addition of *p*-benzoquinone to quench $O_2^{-}\bullet$, signifying that $O_2^{-}\bullet$ was the primary active species for CN^- removal. When EDTA-2Na was added to quench h^+, the CN^- removal efficiency diminished, indicating that h^+ was beneficial in CN^- removal.

Recent study has proved that cyanate (CNO^-) can be generated during the cyanide degradation as a byproduct (Guo et al., 2019). To further explore other compounds used in the CN^-

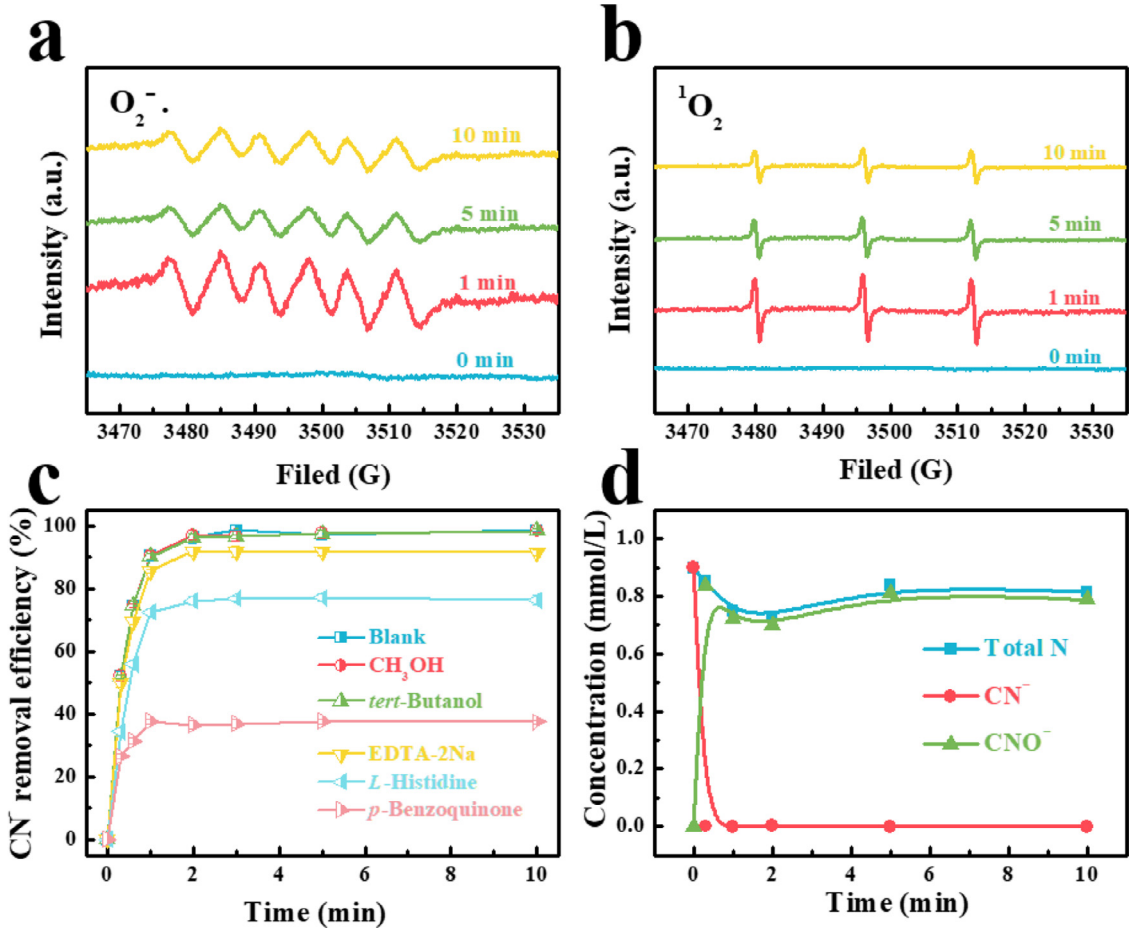

Fig. 3 – Electron paramagnetic resonance (EPR) spectra of (a) O_2^-•, (b) $^1O_2$, (c) quenching experiments results and (d) production of CN^- removal analysis. Reaction conditions: [CN^-] = 44.4 mg/L, applied bias voltage = - 0.5 V, pH = 12.0 and light. EDTA-2Na: ethylenediaminetetraacetic acid disodium salt.

Table 1 – Reactive species and their corresponding rate constant.

Reactive species	Scavenger	Rate constant	References
SO_4^-•	Methanol	~ 10^7	(Wang and Wang, 2020; Clifton and Huie, 1989)
OH	*tert*-Butanol	~ 10^8	Clifton and Huie, 1989
O_2^-•	*p*-Benzoquinone	~ 10^9	Clifton and Huie, 1989
$^1O_2$	*L*-Histidine	~ 10^7	Clifton and Huie, 1989
h^+	EDTA-2Na	~ na	Clifton and Huie, 1989

na: no available; h^+: hole; EDTA-2Na: ethylenediaminetetraacetic acid disodium salt.

removal process, the elements of CN^-, CNO^-, and total nitrogen (TN) were analyzed using UV-vis spectrophotometry and the results are illustrated in Fig. 3d. The initial 44.4 mg/L (0.90 mmol/L) concentration of CN^- was almost completely removed within 2 min, and the concentration of CNO^- rose from 0 to 0.84 mmol/L. The TN content exhibited a slight alteration, showing a downward trend during the initial 2 min, and then gradually rising to almost the original concentration levels. Since the sum of CN^- and CNO^- content was always equal to the amount of TN, it could be reliably stated that the element that was beneficial to the process of CN^- removal was CNO^-. Furthermore, the downward trend displayed by TN during the initial 2 min could have been caused by the adsorption of cathode CA.

It was deduced that the PEC system was beneficial to PMS activation for CN^- removal due to the higher removal efficiency displayed by the PEC/PMS system than that of PMS alone. For determining the impact of photoanode TiO_2 and cathode CA on the activation of PMS, firstly, SEM images and XRD for used TiO_2 were analyzed, with the findings being illustrated in **Figs. S4** and **4a**. No difference was observed in the SEM images and the XRD for fresh and used TiO_2, indicat-

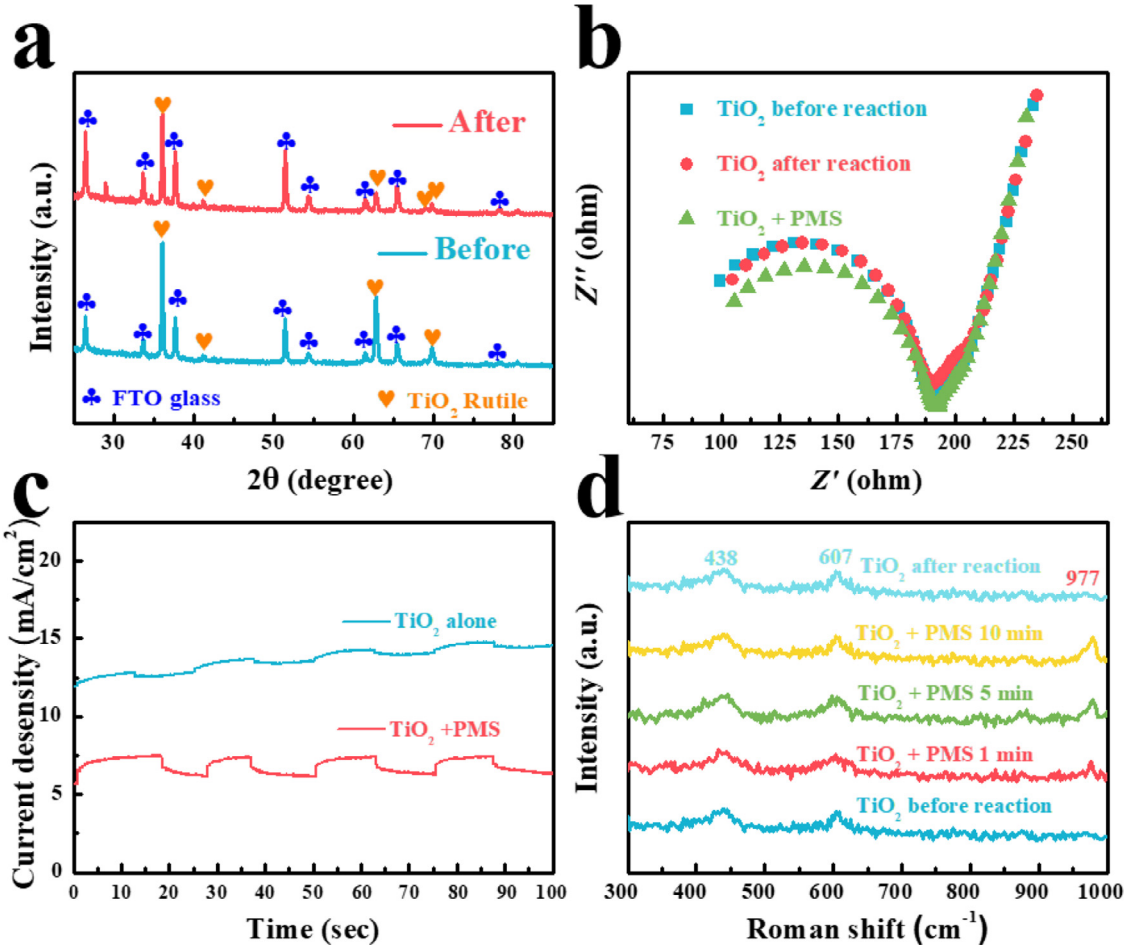

Fig. 4 – (a) X-ray diffraction (XRD) of fresh and used TiO_2, (b) electrochemical impedance spectroscopy (EIS) of TiO_2 in presence of PMS and without, (c) photocurrent density of TiO_2 in presence of PMS and without, and (d) *in-situ* Raman spectra of TiO_2 in presence of PMS and without. Reaction conditions: [PMS] = 0.25 mmol/L, applied bias voltage = -0.5 V, pH = 12.0 and light. FTO: fluorine-doped tin oxide; Z': real parts of the impedance; Z'': imaginary parts of the impedance.

ing the stability of the TiO_2 NRs. Additionally, the EIS of fresh and used TiO_2, and the TiO_2 from the PMS activation process were identified, and the same have been illustrated in Fig. 4b. The radius of the EIS curves of TiO_2 in the presence of PMS is smaller than that of the curves for the fresh and used TiO_2 NRs by themselves. This indicated that a minimal carrier transport resistance occurred after the PMS had been added. Fig. 4c displays the photocurrent density of TiO_2 along with, as well as devoid of, PMS; the photocurrent density of TiO_2 with PMS was higher than that of TiO_2 devoid of PMS. Consequently, TiO_2 and PMS could be combined to improve the separation efficiency of holes and photogenerated electrons, as well as the CN^- removal efficiency.

The *in-situ* Raman test was also used to study the interaction between TiO_2 and PMS, and the findings for the same have been displayed in Fig. 4d. In the presence of only TiO_2, signal peaks appeared at 438 and 606 cm^{-1}, of which 438 cm^{-1} was a O-Ti-O torsional vibration, and 606 cm^{-1} was a O-Ti-O axial anti-symmetric stretching and equatorial bending vibration frequency. With the addition of PMS, peaks were detected at 438, 606, and 977 cm^{-1}, while the peak at 977 cm^{-1} dissipated without PMS. Thus, it could be inferred that the peak of 977 cm^{-1} was O-Ti-O-O-SO_3.

To further investigate the impact that TiO_2 had on PMS activation, the XPS spectrum for used TiO_2 was analyzed (Fig. 5a-c). A new peak formed at nearly 486 eV and was assigned to the K element, which is derived from PMS (Fig. 5a). The peak at 531.6 eV was attributed to the -OH in -Ti(OH)-O-Ti-(OH)- and was enhanced, indicating that additional -Ti(OH)-O-Ti-(OH)- had formed after PMS activation (Fig. 5b). The transformation of O 1s at 531.6 eV could have been caused by the complex formed between TiO_2 and PMS. In addition, a new peak at 532.2 eV was appeared, which could be attributed to the H_2O molecule adsorption on the TiO_2 surface (Hoffmann et al., 1995). The XPS spectrum of Ti remained unchanged (Fig. 5c), indicating the stability of TiO_2.

The influence that the CA cathode had on the activation of PMS was analyzed through a comparison of the CN^- removal efficiency of various CA and Pt cathodes as depicted in **Fig. S5**. The CN^- removal efficiency of the cathode Pt was approxi-

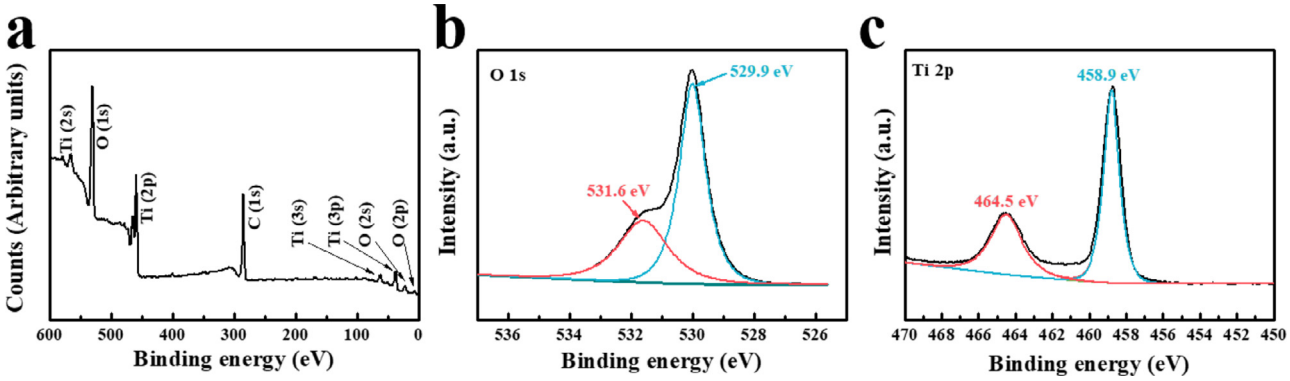

Fig. 5 – (a) X-ray photoelectron spectroscopy (XPS) survey spectrum of used TiO_2 and XPS spectra of (b) O 1s and (c) Ti 2p.

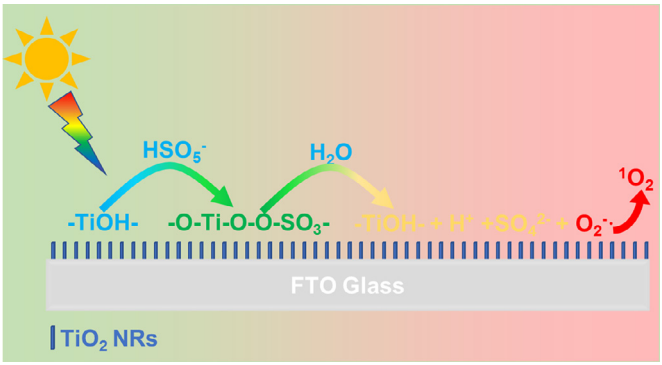

Fig. 6 – Mechanism of PMS activation by TiO_2 nanorods (NRs).

mately 83.4% and was lower than that of the cathode CA. Thus, it could be concluded that the cathode CA positively impacted PMS activation.

Based on the above experiments, a PMS activation mechanism employing TiO_2 was proposed, as in Fig. 6. The surface complex O-Ti-O-O-SO_3 would be formed between PMS and TiO_2 in the presence of light irradiation, which would then be transferred to -TiOH-, $O_2^{-}\bullet$, and SO_4^{2-}. $O_2^{-}\bullet$, undergoing a series of changes to form $^1O_2$. The generation of $O_2^{-}\bullet$ and $^1O_2$ has been denoted in Eqs. (5)–(9) and the possible reactions that could occur in the CN^- removal process have been denoted in Eqs. (10)–(11).

$$TiO_2 + 2H_2O \rightarrow [TiOH]^{3+} + 3OH^- \quad (5)$$

$$HSO_5^- + [TiOH]^{3+} + 2OH^- \rightarrow [O-Ti-O-O-SO_3]^0 + 2H_2O \quad (6)$$

$$[O-Ti-O-O-SO_3]^0 + H_2O \rightarrow [TiOH]^{3+} + HO_2^- \cdot + SO_4^{2-} \quad (7)$$

$$HO_2^- \rightarrow H^+ + O_2^- \quad (8)$$

$$2O_2^- + 2H^+ \rightarrow H_2O_2 + {}^1O_2 \quad (9)$$

$$O_2^- + 2CN^- + H_2O \rightarrow 2CNO^- + OH^- \quad (10)$$

$$^1O_2 + 2CN^- \rightarrow 2CNO^- \quad (11)$$

2.5. *Kinetic analysis and stability test*

In order to analyzed the effect of PEC/PMS system on removal of CN^-, the reaction kinetic constants (k) were calculated using the first-order and second-order dynamics model referred to the previous study (Feng et al., 2020). The removal rate equation can be described as the Eqs. (12) or (13). The curves of CN^- concentration versus time with different initial PMS concentration were obtained and as **Table S1** (first-order) and **Table S2** (second-order). Then the k was calculated and the results as the Table 2.

First-order model:

$$\ln(c_t/c_0) = -k_1 t \quad (12)$$

Second-order model:

$$1/c_t - 1/c_0 = k_2 t \quad (13)$$

where c_t and c_0 are the concentration at time t and the initial concentration, respectively.

The R^2 for the first-order model is consistently higher than that of the second-order model, it was demonstrated that the removal kinetics of CN^- follows the first-order model. The k of PEC/PMS system was increasing with the PMS concentration increased, the reason for that mainly resulting from the more PMS was activated by TiO_2 to forms $O_2^{-}\bullet$ and $^1O_2$. These active species can quickly oxidize the CN^- and achieve the purpose of removing CN^-. Therefore, the PEC/PMS system can be considered as an effective technology to remove cyanide.

Table 2 – Reaction kinetic constants (k) in different peroxymonosulfate (PMS) concentration in photoelectrocatalysis (PEC) system.

System	PMS concentration (mmol/L)	k_1	R^2	k_2	R^2
PEC/PMS	0.10	0.4569	0.8767	0.8375	0.8575
	0.25	0.8671	0.9094	2.8517	0.8914
	0.50	2.2558	0.9882	14.242	0.8440
	1.00	2.6665	0.9894	22.403	0.8902

k_1: k of first-order model; k_2: k of second-order model.

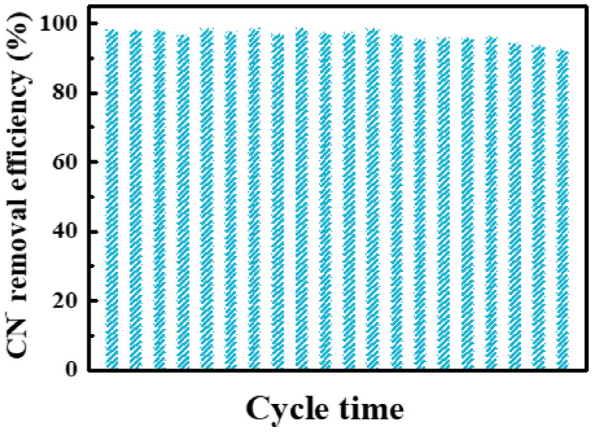

Fig. 7 – Stability analysis of PEC system.

The stability of the catalyst is one of the important indicators in measuring excellence in a pollutant removal system. In this study, the PEC/PMS system was cyclically tested 20 times, with the findings being illustrated in Fig. 7. In this system, the primary function of the TiO_2 photoanode was to activate the PMS by forming a complex on the surface of the TiO_2. The complex was unstable and decomposed into active species, which failed to alter the structure of TiO_2.

3. Conclusions

The PEC system constructed with TiO_2 as the photoelectric anode and CA as the cathode activates the PMS to remove CN^- from wastewater, attaining a removal efficiency as high as 98.5% with light irradiation, an applied bias voltage of -0.5 V, and a PMS concentration of 0.25 mmol/L. The methodology for CN^- removal was analyzed via EPR and quenching experiments, and O_2^{-}• and $^1O_2$ were found to be the dominant active species rather than SO_4^{-}• and •OH. It was also successfully established that PMS was activated by TiO_2 through a comparison using the Raman test, XRD, EIS, and XPS for fresh and used TiO_2. Moreover, this system offers additional advantages such as low cost, technological simplicity, stability of performance, reusability, and broad-spectrum application prospects in the field of water body restoration .

Acknowledgments

This work is supported by the Key projects of National Natural Science Foundation of China (No. 52030003), the National Key R&D Program of China (No. 2019YFC1407800), and sponsored by Joint Doctoral Training Foundation of Hebei University of Technology (HEBUT) .

Appendix A Supplementary data

Supplementary material associated with this article can be found in the online version at doi:10.1016/j.jes.2021.08.054.

REFERENCES

Adams, C.R., Porter, C.P., Robshaw, T.J., Bezzina, J.P., Shields, V.R., Hides, A., et al., 2020. An alternative to cyanide leaching of waste activated carbon ash for gold and silver recovery via synergistic dual-lixiviant treatment. J. Ind. Eng. Chem. 92, 120–130.

Akhavan, O., Ghaderi, E., 2010. Self-accumulated Ag nanoparticles on mesoporous TiO_2 thin film with high bactericidal activities. Surf. Coat. Tech. 204, 3676–3683.

Ao, X.W., Liu, W.J., Sun, W.J., Cai, M.Q., Ye, Z., Yang, C., et al., 2018. Medium pressure UV-activated peroxymonosulfate for ciprofloxacin degradation: Kinetics, mechanism, and genotoxicity. Chem. Eng. J. 345, 87–97.

Chen, F., Liu, L.L., Chen, J.J., Li, W.W., Chen, Y.P., Zhang, Y.J., et al., 2021. Efficient decontamination of organic pollutants under high salinity conditions by a non-radical peroxymonosulfate activation system. Water. Res. 191, 116799.

Chen, X.J., Hua, X.M., Gao, Y., 2019. Removal of NO in simulated flue with aqueous solution of peroxymonosulfate activated by high temperature and Fe(II). Chem. Eng. J. 359, 419–427.

Cho, I.S., Chen, Z.B., Forman, A.J., Kim, D.R., Rao, P.M., Jaramillo, T.F., et al., 2011. Branched TiO_2 nanorods for photoelectrochemical hydrogen production. Nano Lett 11, 4978–4984.

Clifton, C.L., Huie, R.E., 1989. Rate constants for hydrogen abstraction reactions of the sulfate radical, SO_4^{-}. alcohols. Int. J. Chem. Kinet. 21, 677–687.

Deng, J., Xu, M.Y., Qiu, C.G., Chen, Y., Ma, X.Y., Gao, N.Y., et al., 2018. Magnetic $MnFe_2O_4$ activated peroxymonosulfate processes for degradation of bisphenol A: Performance, mechanism and application feasibility. Appl. Surf. Sci. 459, 138–147.

Dong, C.C., Zheng, Z.X., Mohammad A H, B.S., He, J.H., Irene M C, L., 2021. Visible-light-driven peroxymonosulfate activation in photo-electrocatalytic system using hollow-structured

Pt@CeO_2@MoS_2 photoanode for the degradation of pharmaceuticals and personal care products. Environ. Int. 154, 106572.
Duan, W., He, J., Wei, Z., Dai, Z., Feng, C., 2020. A unique Si-doped carbon nanocatalyst for peroxymonosulfate (PMS) activation: insights into the singlet oxygen generation mechanism and the abnormal salt effect. Environ. Sci.: Nano 7, 2982–2994.
Duan, X., Indrawirawan, S., Kang, J., Tian, W., Zhang, H., Sun, H., et al., 2018. Temperature-dependent evolution of hydroxyl radicals from peroxymonosulfate activation over nitrogen-modified carbon nanotubes. Sustain. Mater. Techno. 18, e00082.
Duan, X.G., Ao, Z.M., Zhou, L., Sun, H.Q., Wang, G.X., Wang, S.B., 2016. Occurrence of radical and nonradical pathways from carbocatalysts for aqueous and nonaqueous catalytic oxidation. Appl. Catal. B: Environ. 188, 98–105.
Fan, J., Qin, H., Jiang, S., 2019. Mn-doped g-C_3N_4 composite to activate peroxymonosulfate for acetaminophen degradation: The role of superoxide anion and singlet oxygen. Chem. Eng. J. 359, 723–732.
Feng, S., Xiao, B., Wu, M., Wang, Y., Chen, R.F., Liu, H., 2020. Copper phosphide: a dual-catalysis-center catalyst for the efficient activation of peroxydisulfate and degradation of Orange II. Sep. Purif. Technol. 248, 117004.
Gao, Y., Zhu, Y., Lu, L., Zeng, Q., Xing, X., Hu, C., 2018. Electronic structure modulation of graphitic carbon nitride by oxygen doping for enhanced catalytic degradation of organic pollutants through peroxymonosulfate activation. Environ. Sci. Technol. 52, 14371–14380.
Gao, Y.X., Zhou, Y., Wang, H.T., Lin, W.S., Wang, Y.P., Sun, D.H., et al., 2013. Simultaneous silver recovery and cyanide removal from electroplating wastewater by pulse current electrolysis using static cylinder electrodes. Ind. Eng. Chem. Res. 52, 5871–5879.
Guo, Y.P., Wang, Y.F., Zhao, S., Liu, Z., Chang, H., Zhao, X., 2019. Photocatalytic oxidation of free cyanide over graphitic carbon nitride nanosheets under visible light. Chem. Eng. J. 369, 553–562.
Han, W., Li, D., Zhang, M., Duan, X., Liu, S., Wang, S., 2020. Photocatalytic activation of peroxymonosulfate by surface-tailored carbon quantum dots. J. Hazard. Mater. 395, 122695.
Hoffmann, R., Martin, T., Choi, W., Banhemann, W., 1995. Environmental applications of semiconductor photocatalysis. Chem. Rev. 95, 69–96.
Jawad, A., Zhan, K., Wang, H.B., Shahzad, A., Zeng, Z.H., Wang, J., et al., 2020. Tuning of persulfate activation from a free radical to a nonradical pathway through the incorporation of non-redox magnesium oxide. Environ. Sci. Technol. 54, 2476–2488.
Joa, Y., Kima, C., Moon, G.H., Lee, J., Anc, T.C., Choi, W.Y., 2018. Activation of peroxymonosulfate on visible light irradiated TiO_2 via a charge transfer complex path. Chem. Eng. J. 346, 249–257.
Li, Y., Li, J., Pan, Y., Xiong, Z., Yao, G., Xie, R., et al., 2020. Peroxymonosulfate activation on $FeCo_2S_4$ modified g-C_3N_4 ($FeCo_2S_4$-CN): Mechanism of singlet oxygen evolution for nonradical efficient degradation of sulfamethoxazole. Chem. Eng. J. 384, 123361.
Lv, C.C., Ding, J., Qian, P., Li, Q.C., Ye, S.F., Chen, Y.F., 2015. Comprehensive recovery of metals from cyanidation tailing. Miner. Eng. 70, 141–147.
Mao, R., Di, S., Wang, Y., Zhao, X., 2019. Photoelectrocatalytic degradation of Ag-cyanide complexes and synchronous recovery of metallic Ag driven by TiO_2 nanorods array photoanode combined with titanium cathode. Chemosphere 242, 125156.
Monser, L., Adhoum, N., 2002. Modified activated carbon for the removal of copper, zinc, chromium, and cyanide from wastewater. Sep. Purif. Technol. 26, 137–146.
Qin, J.X., Dai, L., Shi, P.H., Fan, J.C., Min, Y.L., Xu, Q.J., 2020. Rational design of efficient metal-free catalysts for peroxymonosulfate activation: selective degradation of organic contaminants via a dual nonradical reaction pathway. J. Hazard. Mater. 398, 122808.
Sasidharan Pillai, I.M., Gupta, A.K., 2016. Anodic oxidation of coke oven wastewater: multiparameter optimization for simultaneous removal of cyanide, COD and phenol. J. Environ. Manage. 176, 45–53.
Sun, H.Q., Kwan, C., Suvorov, A., Ang, H.M., Tadé, M.O., Wang, S.B., 2014. Catalytic oxidation of organic pollutants on pristine and surfacenitrogen-modified carbon nanotubes with sulfate radicals. Appl. Cata. B: Environ. 155, 134–141.
Song, X.L., Liu, M.Q., 2018. Advanced treatment of biotreated coking wastewater with peroxymonosulfate oxidation catalyzed by granular activated carbon. J. Chem. Technol. Biot. 93, 2191–2198.
Sun, M., Chu, C.H., Geng, F.L., Lu, X.L., Qu, J.H., Crittenden, J., et al., 2018. Reinventing Fenton chemistry: Iron oxychloride nanosheet for pH insensitive H_2O_2 activation. Environ. Sci. Technol. Lett. 51, 86–191.
Tian, S.C., Dang, C.Z., Mao, R., Zhao, X., 2018. Enhancement of photoelectrocatalytic oxidation of Cu-cyanide complexes and cathodic recovery of Cu in a metal-free system. ACS Sustain. Chem. Eng. 6, 10273–10281.
Tian, S.C., Li, Y., Zeng, H., Guan, W., Wang, Y., Zhao, X., 2016. Cyanide oxidation by singlet oxygen generated via reaction between H_2O_2 from cathodic reduction and $OCl^{(-)}$ from anodic oxidation. J. Colloid. Interf. Sci. 482, 205–211.
Wang, J.L., Wang, S.Z., 2018. Activation of persulfate (PS) and peroxymonosulfate (PMS) and application for the degradation of emerging contaminants. Chem. Eng. J. 334, 1502–1517.
Wang, N., Ma, W., Ren, Z., Du, Y., Xu, P., Han, X., 2018. Prussian blue analogues derived porous nitrogen-doped carbon microspheres as high-performance metal-free peroxymonosulfate activators for non-radical-dominated degradation of organic pollutants. J. Mater. Chem. A 6, 884–895.
Wang, J.L., Wang, S.Z., 2020. Reactive species in advanced oxidation processes: Formation, identification, and reaction mechanism. Chem. Eng. J. 401, 126158.
Wang, Y., Zhao, G., Chai, S., Zhao, H., Wang, Y., 2013. Three-dimensional homogeneous ferrite-carbon aerogel: one pot fabrication and enhanced electro-Fenton reactivity. ACS Appl. Mater. Interf. 5, 842–852.
Wang, Y.F., Tian, S.C., Cao, D., Wang, Y.B., Wang, Y., Qiao, M., et al., 2017. Enhancement of electrochemical oxidation of $Cu(CN)_3^{2-}$ by the peroxydisulfate oxidation. Sep. Purif. Technol. 188, 119–125.
Xie, Y.R., Wei, L., Wei, G.D., Li, Q.H., Wang, D., Chen, Y.X., et al., 2013. A self-powered UV photodetector based on TiO_2 nanorod arrays. Nanoscale. Res. Lett. 8, 188.
Yang, X.J., Xu, X.M., Xu, J., Han, Y.F., 2013. Iron oxychloride (FeOCl): an efficient Fenton-like catalyst for producing hydroxyl radicals in degradation of organic contaminants. J. Am. Chem. Soc. 135, 16058–16061.
Ye, J., Cheng, H., Li, H., Yang, Y., Zhang, S., Rauf, A., et al., 2017. Highly synergistic antimicrobial activity of spherical and flower-like hierarchical titanium dioxide/silver composites. J. Colloid. Interf. Sci. 504, 448–456.
Zheng, Y., Li, Z.K., Wang, X.Y., Gao, X.L., Gao, C.J., 2015. The treatment of cyanide from gold mine effluent by a novel five-compartment electrodialysis. Electrochim. Acta. 169, 150–158.
Zhu, S.H., Li, X.J., Kang, J., Duan, X.G., Wang, S.B., 2019. Persulfate activation on crystallographic manganese oxides: Mechanism of singlet oxygen evolution for nonradical selective degradation of aqueous contaminants. Environ. Sci. Technol. 53, 307–315.